ACS OMEGA

http://pubs.acs.org/journal/acsodf

Article

Acting as a Molecular Tailor: Dye Structural Modifications for Improved Sensitivity toward Lysophosphatidic Acids Sensing

Nicolas Fontaine, Lara Harter, André Marette, and Denis Boudreau*

Cite This: *ACS Omega* 2023, 8, 1067−1078

Read Online

ACCESS | Metrics & More | Article Recommendations | Supporting Information

ABSTRACT: Lysophosphatidic acids (LPA) are key biomarkers for several physiological processes, the monitoring of which can provide insights into the host's health. Common lab-based techniques for their detection are cumbersome, expensive, and necessitate specialized personnel to operate. LPA-sensitive fluorescent probes have been described, albeit for nonaqueous conditions, which impedes their use in biological matrices. In this paper, we explore in detail the influence of structure on the extent of aggregation-induced fluorescence quenching using specially synthesized styrylpyridinium dyes bearing structural adaptations to bestow them enhanced affinity toward LPA in aqueous media. Spectroscopic investigations supported by time-resolved fluorimetry revealed the contribution of excimer formation to the fluorescence quenching mechanism displayed by the fluorescent probes. Experimental observations of the influence of structure on detection sensitivity were supported by DFT calculations

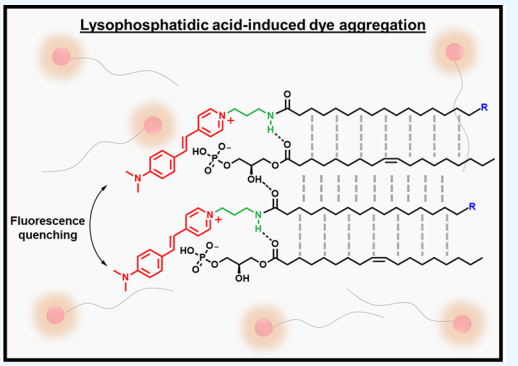

INTRODUCTION

Health professionals rely on biomarker monitoring to ensure disease identification and treatment at early stages of development to improve the cure success rate.[1,2] Biomarker sensing has been a popular avenue of research in recent years since the progress in technology allows for a more thorough characterization of complex matrix constituents and deciphering their relationship with the host health.[3−8] Considering the plethora of compounds found *in vivo*, determining species involved in several physiological processes can be advantageous in limiting the number of analyses required.

In 1963, W. Vogt demonstrated the importance of lysophosphatidic acids (LPAs) as bioactive compounds by showing their effect on the contraction of the duodenum in rabbits.[9] Since LPAs are found in several biological fluids ranging from plasma, intestinal mucosa, and even the aqueous humor, this discovery resulted in a growing interest to elucidate the origin of these phospholipids as well as their principle of action.[10,11]

LPAs are the simplest phospholipids and consist of a phosphate group, a glycerol spacer, and a hydrophobic chain of variable size with or without the presence of unsaturations.[12] One of the most common, LPA 18:1, is shown as an example in Figure 1.

LPAs are known to be mediators in cell migration and in the formation of blood vessels to enable wound healing through the activation of G-protein transmembrane receptors.[10,13−16] Articles reporting on the nominal concentration of LPA in plasma show a relatively large window ranging from below 0.1 μM up to nearly 150 μM.[17−20] According to the group of Kano et al. who recently investigated the potential causes of these major discrepancies,[21] this variability comes from poor sample storage procedures which leads to the continuation of the metabolic production of LPA as well as their degradation *ex vivo*. By lowering the storage temperature and adding to the samples an inhibitor of autotaxin (ATX), a water-soluble protein involved in the biosynthesis of LPA, they determined a range of 40−50 nM for LPAs in humans. Over the years, LPA determination in biological fluids has made it possible to establish links between the concentration of LPAs and the appearance of certain diseases or cancers. Increased amounts of LPAs are linked to various diseases from aortic atherosclerosis,

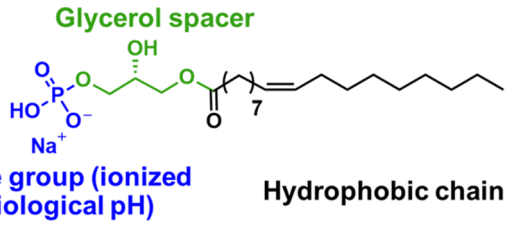

Figure 1. Chemical structure of lysophosphatidic acid 18:1.

Received: October 4, 2022
Accepted: December 13, 2022
Published: December 28, 2022

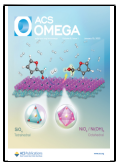

peritoneal, endometrial, and cervical carcinoma as well as colon and ovarian cancers.[17,18] This makes LPAs a biomarker of high interest in health care.

The most common approaches to determine the amount of LPA in biological fluids are based on chromatography coupled to mass spectrometry.[22] Despite their benefits in terms of sensitivity and analytical throughput, these methods require highly trained personnel and are cumbersome, time-consuming, and expensive to operate. In recent years, researchers pushed the boundaries of LPA sensing by developing molecular probes that can be used with optical techniques such as colorimetry and spectrofluorimetry. The latter is well known for its high sensitivity, lowered costs of instrumentation,[23] and has been applied to target detection directly in complex biological matrices.[24−27]

Reported fluorometric probes for LPA sensing exploit several transduction mechanisms ranging from enzymatic reaction with LPA to produce a fluorescent species,[28] polarity changes,[29] competition assays,[30,31] and conformational changes in polymeric structure.[32] The most popular approach consists in using fluorescent probes having a structure that is complementary to that of LPAs to induce aggregation upon interaction with the target (Figure 2).[22,33−35] This aggregation

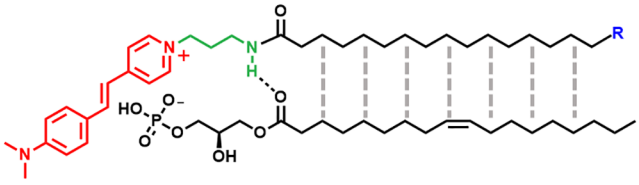

Figure 2. Expected interaction of the developed probes with LPA 18:1.

causes fluorescence changes in the form of quenching or enhancement, depending on the spectral properties of the probes, and good selectivity is often reported for this technique. However, to the best of our knowledge, there are no exhaustive study on the impact of structure complementarity toward LPA detection. In the work presented herein, we synthesized several structural variants of a previously reported styrylpyridynium fluorescent probe to determine the influence of structure on sensitivity, in particular the length of the hydrophobic end chain, in addition to three different end groups often used for immobilization on solid substrates (Figure 3).

RESULTS AND DISCUSSION

Dye Concentration and Effect of pH. From the three end groups added to the dye structures, i.e., NHS, silane, and azide (Figure 3B), the azide offers improved stability toward degradation compared to the potential hydrolysis of the two others in aqueous conditions. The azido-bearing compounds were therefore used for mechanistic investigations regarding LPA detection. Fluorescence spectra were recorded for two concentrations of Fluo-N_3 (1.4 and 14.2 μM) as a function of the concentration of LPA present in the medium (Figure 4A). For the lower probe concentration, the fluorescence band attributed to DSHP decreases rapidly before increasing again while remaining in a similar wavelength range. At higher probe concentrations, an initial decrease of the emission band is also present, but is followed by the appearance of a band at a higher wavelength. The generation of this broader band coincides with the visually observable formation of macroscopic aggregates in the cell. This phenomenon was not observed in the previous report, a discrepancy that could be due to different solvent conditions (30% aqueous EtOH as opposed to HEPES hence herein).[34] Moreover, the onset of this phenomenon occurs at a lower LPA concentration than the critical micellar concentration (CMC) determined for this system (220 μM, Supporting Information, Figure S6), and thus cannot be ascribed to the formation of LPA micelles. Moreover, it can be postulated that micelle formation would allow better solubilization of the fluorophores and therefore prevent the formation of aggregates.

These aggregates, although allowing detection with the naked eye above a certain threshold in LPA concentration, are disadvantageous in terms of fluorescence transduction given the higher background signal generated by the heterogeneity of the mixture. A lower probe concentration was thus employed throughout the rest of the experiments, acknowledging the fact that they are more sensitive toward fluorescence quenching in these conditions (Figure 4B). These results are supported by spectrophotometric studies showing no signs of dye microscopic aggregates in the absence of LPA and a more significant signal change of the extinction spectra with LPA for lower dye concentration (Supporting Information, Figures S7 and S8).

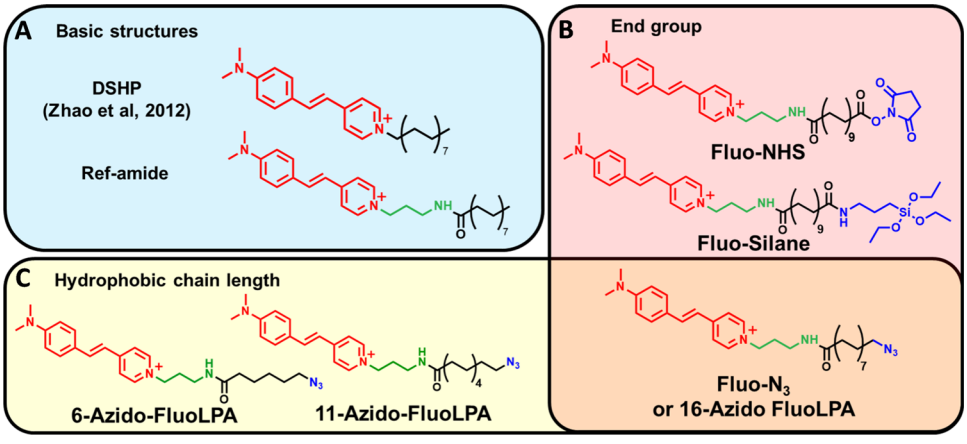

Figure 3. Fluorescent probes synthesized for the comparative study on LPA sensing.

https://doi.org/10.1021/acsomega.2c06420
ACS Omega 2023, 8, 1067−1078

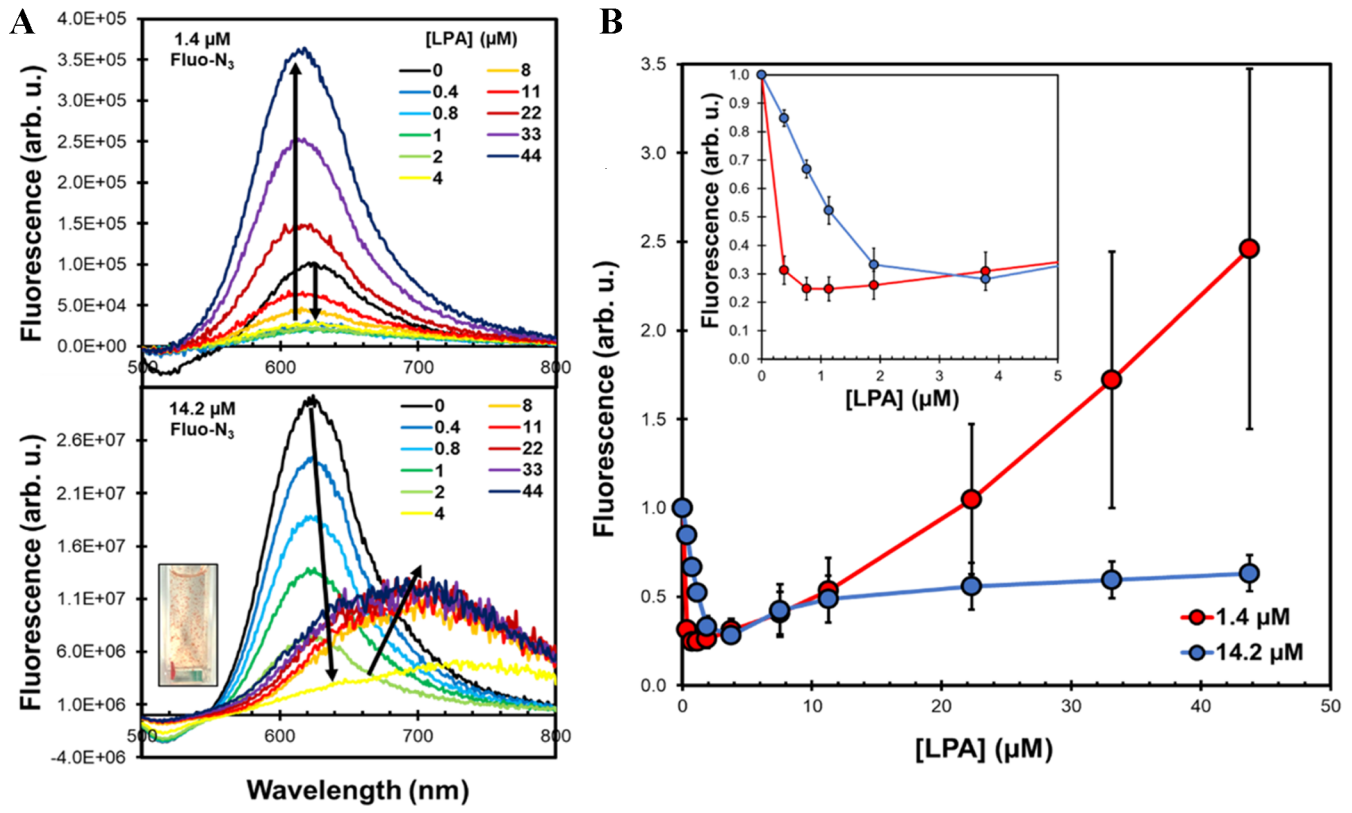

Figure 4. Fluorescence spectra for two concentrations of Fluo-N_3 during calibration with LPA in 10 mM HEPES buffer, pH 7.4 containing 0.07 and 0.7% MeOH for 1.4 and 14.2 μM dye, respectively (A), and related calibration curves (B). Inset: Emphasis on the 0−5 μM range of LPA. λ_{ex} = 480 nm, slits = 5 nm, fluorescence signal integrated from 575 to 800 nm, n = 3.

For a given concentration of dye in the analysis medium, the addition of low amounts of LPA induces dye aggregation, which leads to fluorescence quenching. However, when an excess of LPA is reached, the observed fluorescence recovery could come from the destabilization of the aggregates by LPA molecules, separating the dye molecules from each other even if the concentration is significantly lower than the CMC. The pH also affects the probes' response (Supporting Information, Figure S14) as the fluorescence quenching and intensity of the lower-energy broad band show high variability for each of the studied probes. It is important to note that Britton−Robinson buffers were used instead of HEPES for this test to provide a finer control on the pH of the solutions and that the different chemical makeup of the two buffers could explain the differences observed with the results in HEPES. As LPA are biologically relevant compounds, 10 mM HEPES buffer (pH 7.4) was used throughout the following characterizations.

The decrease of the band at 620 nm in favor of the appearance of a broader band at higher wavelength suggests the formation of an excimer and the disappearance of the monomer.[41,42] Furthermore, the stabilization of the band at ∼700 nm suggests that at these and higher LPA concentrations, all of the available probes already interact within the aggregates, thus preventing any further increase in signal.

Time-Resolved Fluorescence and Kinetic Experiments. To validate the hypothesis of excimer formation, time-resolved spectrofluorimetry analysis was performed (Figure 5).

The exponential decay curve of Fluo-N_3 alone in HEPES is narrow and barely stands out from the instrumental response function obtained with a suspension of silica nanoparticles.

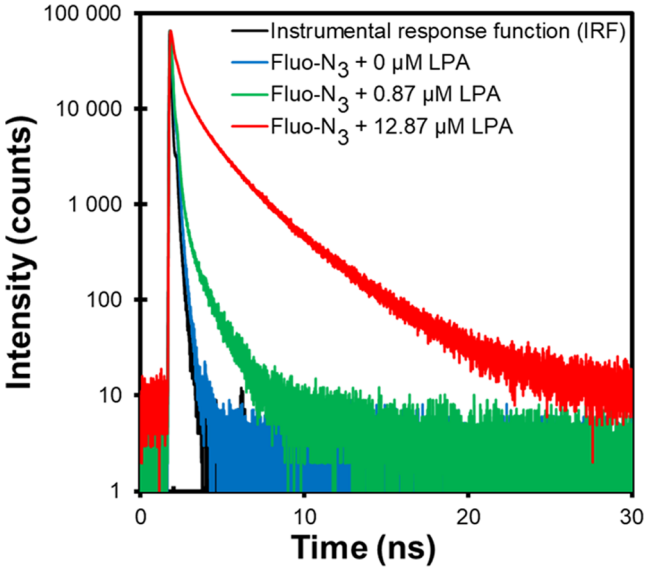

Figure 5. Multiexponential decay curves for Fluo-N_3 (3.3 μM) as a function of LPA concentration in 10 mM HEPES buffer, pH 7.4 containing 0.7% MeOH. The instrumental response function (IRF) was determined with a silica nanoparticle suspension. λ_{ex} = 475 nm, λ_{em} = 615 nm, slits = 2 mm, n = 1.

The addition of LPA in the medium induced a significant increase in the counts accumulated for longer times, thus resulting in an increase in the average lifetime. The exponential decay data were fitted with either a two- or three-component

https://doi.org/10.1021/acsomega.2c06420
ACS Omega 2023, 8, 1067−1078

Table 1. Lifetime Decay Exponential Curve Fitting Results for Fluo-N3 in the Presence of LPA

[LPA] (μM)	τ_1 (ns)/weight (%)	τ_2 (ns)/weight (%)	τ_3 (ns)/weight (%)	τ_{ave} (ns)	X^2
0	0.04/90	0.10/10	NA	0.05	1.656
0.87	0.05/96	0.22/3	1.13/1	0.06	1.280
12.87	0.12/76	0.94/19	2.96/5	0.44	1.820

exponential curve as dictated by the resulting goodness of fit (χ^2) (Table 1) according to eq 1

$$I(t) = \int_{-\infty}^{t} \mathrm{IRF}(t') \sum_{i=1}^{n} A_i e^{-t-t'/\tau_i} \, dt' \quad (1)$$

where I is the number of counts, t is time, IRF is the instrumental response function, A_i is the amplitude or weight of component i, and τ_i is the component-related fluorescence lifetime.

In the absence of LPA, a short component (40 picoseconds) with 90% amplitude weight is obtained, and can be assigned to source light scattered in the sample cell and routed to the PMT detector. The longer component (100 ps) was assigned to the fluorescent decay of the molecular probe. The addition of LPA in the solution caused the appearance of a third component having a lifetime an order of magnitude greater than that for the lone probe. This longer component also increased from 1.13 to 2.96 ns when going from 0.87 to 12.87 μM of LPA, with a weight proportional to the amount of LPA added. This study was repeated with Fluo-Silane with an emission wavelength of 610 and 700 nm in an attempt to separate the contributions of the "monomers" and the excimers (Supporting Information, Figure S10). However, signal cross-talk due to the width of the bands in the selected channels causing a linear trend of the mean lifetime over the range from 0 to ~60 μM for the monochromator set at 610 nm. The band at 600 nm is narrower and has a weaker contribution at 700 nm, which would explain the initial increase in the average lifetime before some stabilization for the highest concentration of LPA tested.

Mishra et al. reported a detailed study of derivatives possessing the same fluorescent head as the one used in this research.[43] They varied the carbon chain length with small increments and compared the absorption spectra as well as the fluorescence lifetime values in different solvents as well as in the presence of a surfactant (sodium dodecyl sulfone, SDS). An average lifetime of 0.09 ns was determined for DSHP in water, similar to the value of 0.1 ns obtained in this work for Fluo-N_3 in HEPES buffer. Moreover, a directly proportional increase in lifetime was also observed with increasing SDS in the medium, thus agreeing with the results presented here with the addition of LPA.

At lower concentrations of fluorophores, no band was observed at higher wavelengths. This could be caused by the excess LPA, which destabilizes the interaction with the fluorophores without there being enough probes, and therefore an adequate distance, for the formation of excimers. To reduce the uncertainty brought by the formation of insoluble aggregates, a fluorophore concentration of 0.3 μM was chosen for subsequent experiments in HEPES buffer. Examination of the fluorescence spectrum in the presence of LPA or in different organic solvents (Supporting Information, Figures S11–S12) suggests that LPAs do not induce significant changes in local polarity and thus would not contribute to the detection mechanism.

Time-resolved measurements in 10 mM HEPES buffer solutions containing 0 and 30% EtOH revealed differences in fluorescence signal stability (Supporting Information, Figure S13). Dyes in the buffer with 30% EtOH show good signal stability over several minutes, whereas a significant decrease was observed in pure aqueous buffer, with a quenching of around 20% over 2 min. This suggests a poor solubility of the probes in aqueous conditions and their aggregation over time. For both buffer compositions tested, the addition of LPA induced a rapid and significant fluorescence change spanning only over a few tens of seconds, which could be exploited in dynamic sensing schemes.

Effect of Dye Structure and Analysis Medium. The majority of fluorescent probes previously reported for the detection of LPA possess a perfectly complementary structure with the molecular target, i.e., a cationic moiety positioned at the end of a hydrophobic chain. On an individual basis, the interaction between ionic charges is significantly stronger than that between hydrophobic groups (van der Waals forces). However, the additive aspect of the latter makes it possible to increase their contribution, leading to the development of probes having a high affinity toward the molecular target. In this regard, Zhao et al.[34] compared the original DSHP probe to one having the same cationic head, but its hydrophobic chain is replaced by an allyl group. The probe without a hydrophobic chain showed a lower sensitivity toward LPA compared to DSHP, a result supporting the importance of electrostatic complementarity.[34]

We synthesized three fluorescent probes having hydrophobic chains of 6, 11, and 16 carbons, respectively (Figure 3C) to evaluate the importance of the hydrophobic effect on the detection of LPA (Figure 6).

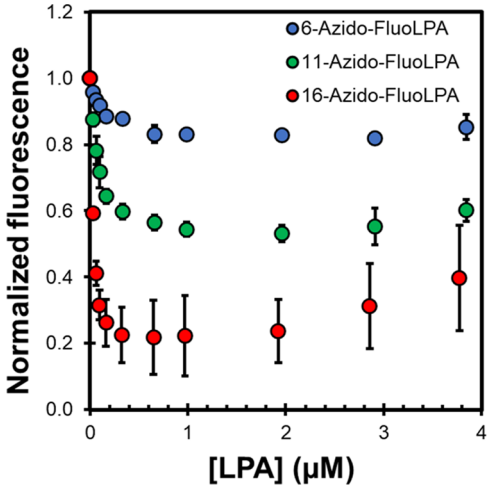

Figure 6. Calibration curves for three DSHP derivatives (see main text) at 0.3 μM in the presence of LPA in 10 mM HEPES buffer, pH 7.4 containing 0.07% MeOH. λ_{ex} = 470 nm, slits = 8 nm, fluorescence integrated from 540 to 800 nm, n = 2.

https://doi.org/10.1021/acsomega.2c06420
ACS Omega 2023, 8, 1067−1078

The results show a clear trend between the different carbon chain lengths. The 16-Azido-FluoLPA derivative exhibits fluorescence quenching (~80%) from 0 to 300 nM of added LPA, compared to ~10 and ~40% for the 6- and 11-carbon derivatives, respectively. The hydrophobic effect therefore appears to play an important role in the sensitivity of LPA probes. At LPA concentrations above 300 nM, the signal seems to reach a plateau while losing in precision, thus limiting the applicability of the sensors at higher concentrations. On the other hand, the dynamic range of this fluorescence quenching phenomenon can be tailored by modifying the probe concentration, as suggested by the results in Figure 4.

The different hydrophobic chain-bearing probes were compared under the same conditions (solvent, probe concentration) to determine whether certain molecular structures stand out in terms of sensitivity. First, a calibration was carried out under the same conditions as the reference article, i.e., in a 10 mM HEPES buffer, pH 7.4 with 30% EtOH and 20 μM of probes (Figure 7). It can be postulated that the addition of an organic solvent in the medium prevents the formation of insoluble aggregates in the range of concentrations tested.

The species showing the most significant fluorescence quenching for these conditions are DSHP and Fluo-NHS. The lower solubility of these compounds could explain the results because the hydrophobic chain alone or a compound bearing an NHS group is generally poorly soluble in water. The addition of LPA therefore more easily causes the formation of a compact arrangement or aggregates with the probes. Unexpectedly, the addition of an amide group on the structure to promote the interaction of the probes with the glycerol portion of LPA does not seem to improve sensitivity. The effect of the addition of a single hydrogen bridge would therefore be negligible in the total interaction with the LPAs in comparison with the ionic charge and the additive aspect of the van der Waals forces with the hydrophobic chain. It is also possible to observe that the exponential decay trend continues over the entire range of LPA concentrations in the μM range. In addition to varying the concentration of fluorescent probes, the dynamic range can also be extended by changing the composition of the solvent. This information is particularly useful for sensing applications that can be completed under nonphysiological conditions.

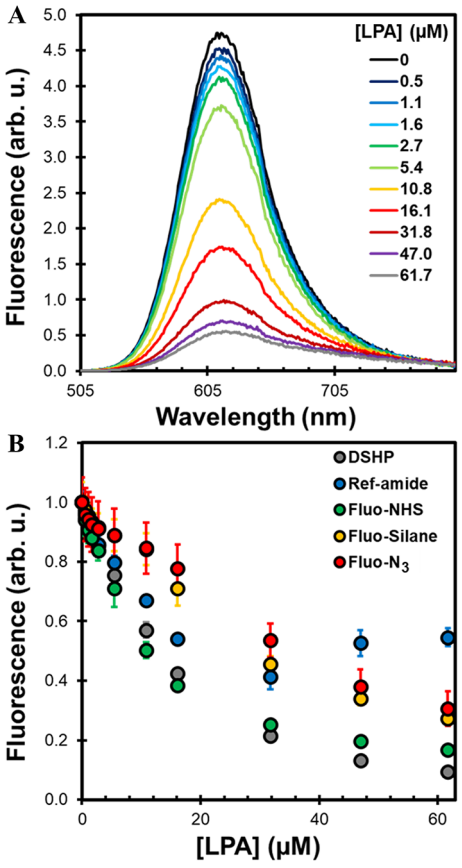

Figure 7. Fluorescence spectra of Fluo-NHS (20 μM) as a function of [LPA] added in 10 mM HEPES buffer, pH 7.4 containing 30% EtOH (A) and related calibration curves for each of the tested probes for comparison (B) (λ_{ex} = 476 nm, slits = 2 nm, fluorescence integrated from 500 nm to 800 nm, n = 3 for DSHP, Ref-amide, Fluo-NHS and Fluo-Silane, n = 2 for Fluo-N_3).

We wanted to test our sensors in a purely aqueous HEPES buffer as a step toward more representative physiological conditions. Since the sensitivity of the probes is higher in aqueous environments, the calibration was carried out in the nanomolar range for easier comparison between the different probes (Figure 8). It should also be noted that a probe concentration of 0.3 μM was used to limit the formation of insoluble aggregates during the experiments.

Different trends were observed for the different fluorescent probe derivatives. In the case of DSHP, an increase in fluorescence is initially observed along two distinct slopes, contrary to the mechanism proposed of an initial extinction of fluorescence. It is possible that the lack of solubility of the probe in HEPES buffer causes the formation of small aggregates which, initially, are destabilized by the LPA. The lowest sensitivity was observed for the Ref-amide derivative, which exhibits minimal fluorescence quenching below 200 nM.

The probes bearing a functional end group exhibit fluorescence quenching of approximately 75% in the range of 0−200 nM. The data were treated using the Stern−Volmer equation (eq 2) to generate linear relationships of the trends obtained (Figure 9).

$$\frac{F_0}{F} = 1 + k_q \tau_0 [Q] \tag{2}$$

where F_0 is the fluorescence without quencher, F with quencher, k_q is the quenching constant, τ_0 the fluorescence lifetime without quencher, and $[Q]$ is the quencher concentration. The detection limits were then calculated from these Stern−Volmer curves according to

$$\text{LOD} = \frac{b + 3\sigma_b}{m} \tag{3}$$

where b is the y-intercept, σ_b is the y-intercept uncertainty, and m is the slope.

Correlation coefficients greater than 0.99 were obtained for the probes with end groups. The detection limits (LOD) calculated from these results are in the order of 47, 36, and 28 nM for Fluo-N_3, Fluo-Silane, and Fluo-NHS, respectively. These values are 1−2 orders of magnitude lower than the detection limits usually reported for this type of system.[34,35]

Selectivity and Interference Studies. The development of sensitive sensors allowing direct detection of targets within complex matrices is important to overcome the limitations of common lab-based methods. The selectivity of Fluo-NHS was

https://doi.org/10.1021/acsomega.2c06420
ACS Omega 2023, 8, 1067−1078

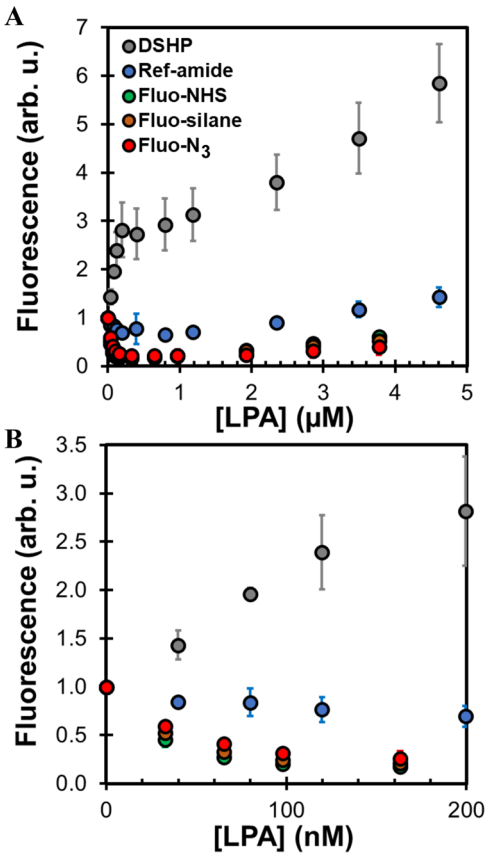

Figure 8. Calibration curves for 0.3 μM of each of the probes in 10 mM HEPES buffer, pH 7.4 containing 0.07% of MeOH for an LPA concentration range of (A) 0−5 μM and (B) 0−200 nM. Analysis parameters are as follows for DHSP, Ref-amide, Fluo-NHS, Fluo-Silane, and Fluo-N_3, respectively: λ_{ex} = 460, 476, 485, 485, 485 nm, slits = 8, 6, 7, 7, 7 nm, fluorescence integrated in the ranges 550−800, 500−800, 550−800, 520−800, and 520−800 nm, n = 3 for DSHP, Ref-amide, Fluo-NHS, and Fluo-Silane, n = 2 for Fluo-N_3.

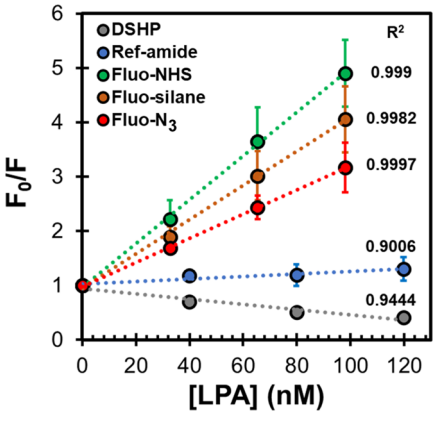

Figure 9. Data from Figure 8 represented in accordance with the Stern−Volmer theory.

investigated by exposing it to different concomitant species: ions, small molecules, and proteins. Fluo-NHS was selected since it is the probe offering the best detection performance compared to the two other derivatives having a reactive group at the end.

The results presented in Figure 10 show that the Fluo-NHS fluorescence undergoes quenching in the order of 20% for the

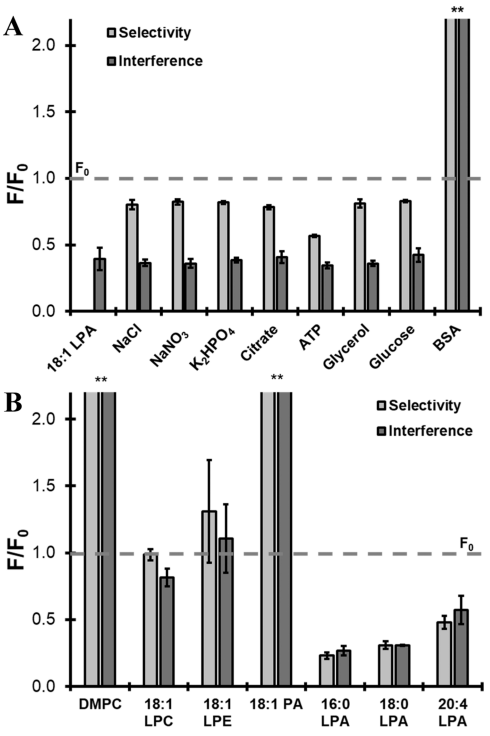

Figure 10. Selectivity and interference studies for LPA sensing with 0.3 μM Fluo-NHS in 10 mM HEPES buffer, pH 7.4 containing 0.07% MeOH in the presence of 1 μM ions, small molecules, and 1 μg/mL proteins (A) and 1 μM species structurally similar to LPA (B). λ_{ex} = 470 nm, slits = 8 nm, fluorescence integrated from 550 to 800 nm, n = 3; ≪ ** ≫ symbols correspond to species that have caused a significant increase of fluorescence instead of the expected quenching. Clipping of these bands allows us to put emphasis on the latter. Dashed lines identified as "F_0" represents the fluorescence measured without added analyte and thus correspond to a stable signal when adding other species.

small molecules and ions tested, except for ATP. The addition of LPA to the medium, however, makes it possible to find a constant fluorescence quenching of approximately 60% of the initial signal. In the case of bovine serum albumin (BSA), a rather significant amplification of the signal was observed and can be attributed to the insertion of the probe into the hydrophobic domains of the protein. This is in line with data acquired previously in solvents of different polarities (Supporting Information, Figure S7).

Unfortunately, articles describing this type of sensor generally do not compare the response of the probes with molecular species structurally similar to LPAs. Different variants of LPAs are also often ignored in favor of the 18:1 LPA commonly used as a model. We therefore performed experiments for a series of common LPAs in addition to other similar structures such as phosphatidic acid (PA), lysophosphatidylethanolamine (LPE), lysophosphatidylcholine (LPC), and dimerystilphosphatidylcholine (DMPC) (Figure 10B).

Fluorescence analysis in the presence of structurally similar derivatives gave more contrasted readings. DMPC and PA gave significantly enhanced fluorescence signals, potentially attributable to the low solubility of these species in HEPES buffer and therefore more prone to form micelles. LPC and LPE, although not showing significant differences with the reference signal, cause interference in the detection of LPA and do not allow significant LPA detection for LPE.

https://doi.org/10.1021/acsomega.2c06420
ACS Omega 2023, 8, 1067−1078

The different structures of LPA, varying according to the length of the hydrophobic chain as well as the number of unsaturations, showed more significant fluorescence quenching. Saturated LPAs induced the greatest signal change and the addition of the 18:1 LPA did not further quench the fluorescence. A similar trend was observed for LPA 20:4, although fluorescence quenching was not as significant as for the other derivatives. The fact that there is no change induced upon addition of the target in the presence of the LPA interferents potentially indicates that the probe has fully interacted with the interferent, preventing a signal change with the addition of more LPA. Similar trends were also obtained for the experiments with Fluo-Silane and Fluo-N_3 (Supporting Information, Figure S15).

These results suggest that hydrophobic compounds present in significant amounts in the sample matrix would be detrimental to the detection of specific LPA species; nevertheless, these results show that the fluorescent probes studied in this work have the potential to perform the quantification of total LPA following removal of the potential interferents.

Computational Results. To support our comparative analysis of the probes developed in this work, we investigated the structures as well as the thermochemistry of the association of the different fluorophores with lysophosphatidic acids using the density functional theory (DFT). We performed the calculations in water as an approximation of HEPES buffer. Thus, a possible specific interaction between the probe and HEPES molecules could alter the thermodynamics of the reactions in our experimental conditions and cause discrepancies between the calculations and the titration results. Moreover, while the calculations were performed by considering one dye and one target molecule, it is expected that several probes and LPA species can be involved in the formation of one aggregate.

We found that several possible LPA conformers are possible, including an open and a closed form (Figure 11).

The open form is caused by the surfactant nature of the lysophosphatidic acid. Indeed, to limit the interaction of the hydrophobic tail with water molecules, the LPA will tend to position itself at the air−water interface in an ordered manner with the tail in a linear conformation.[44,45] However, there are still some molecules in solution with a random orientation. The closed form is due to the polarity of the solvent which causes the hydrophobic chain of the LPA to fold onto itself.[46] Comparison of the open and closed LPA forms shows a Gibbs free energy (ΔG) difference of 3.8 kcal/mol favoring the open conformation in water. Knowing this, only the open conformation was considered for the calculations with the fluorophores. The choice of this conformation was prioritized here because of its stability and because the experiments were carried out at LPA concentrations below the critical micellar concentration, which favors the open conformation in solution. It is however possible that the closed form interacts with the sensors, as a value of 3.8 kcal/mol indicates a reversible process that can also be affected by the compounds added to the characterized medium. For the fluorophore, the simplest conformation was used; however, several other conformers are possible. A more in-depth analysis would then be necessary to confirm the most stable species as well as to obtain the reaction mechanisms.

The calculated structures (Supporting Information, Figures S24−S30) show a linear arrangement arising in part from the hydrophobic effect between the carbon chains of the two molecules. Moreover, ΔG values for the association reaction indicate that all of the interactions between the two molecules are favored (Table 2).

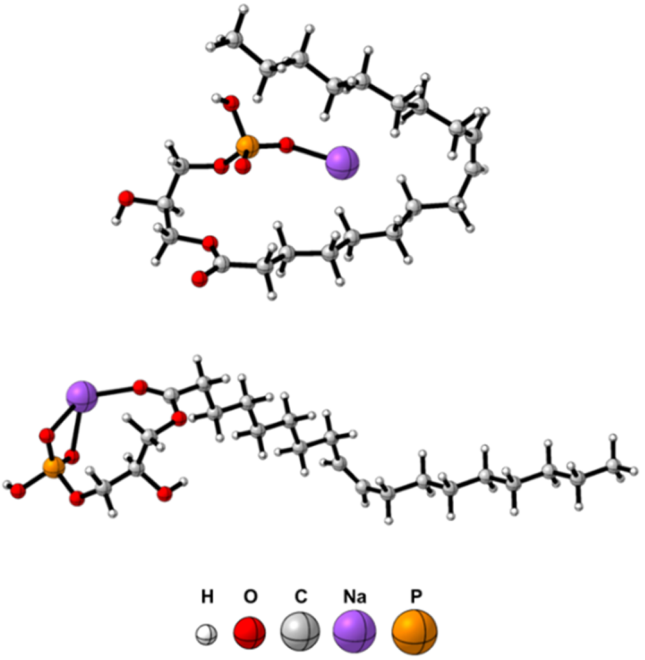

Figure 11. Different conformations of lysophosphatidic acid (open form, top, and closed form, down) in water, calculated at the ωB97XD/6-311G(d,p) (SMD = water) level of theory.

Table 2. Variation of Gibbs Free Energy (ΔG) and Standard Enthalpy (ΔH) for the Different LPA/Fluorophore Associations Calculated at the ωB97XD/6-311G(d,p) (SMD = water) Level of Theory

fluorophore interacting with LPA 18:1	ΔG (kcal/mol)	ΔH (kcal/mol)
Fluo-Silane	−12.1	−32.9
DSHP	−7.1	−17.7
11-Azido-FluoLPA	−5.8	−18.5
Ref-amide	−5.7	−18.5
Fluo-NHS	−3.4	−21.1
16-Azido-FluoLPA	−3.3	−19.1
6-Azido-FluoLPA	0.0	−13.6

On the other hand, the interactions between the silane and the LPA are more favorable than for the other molecules. This stronger interaction can be explained by a greater destabilization of the molecule in water due to the hydrophobic silane group, thus promoting the arrangement of the two molecules. For the same reason, the ΔG values of two of the three azido groups would be closer to 0 given the higher polarity of the azide allowing better stability in water. Finally, the carbon chain length of the azido species (16-Azido-FluoLPA, 11-Azido-FluoLPA, and 6-Azido-FluoLPA) has an impact on the Gibbs free energy value. Indeed, a chain with a carbon number equivalent to the lysophosphatidic chain would be more favored over longer or shorter chains. This difference can be rationalized by a better stacking between the two molecules, leading to better stabilization instead of having a potential destabilization caused by the solvent "icelike" structure around the remaining carbons of the chain.

https://doi.org/10.1021/acsomega.2c06420
ACS Omega 2023, 8, 1067−1078

It can be observed that the computational results agree rather poorly in general with the experimental results. To begin with, as discussed, the optimal chain length determined by DFT is 11 carbons (based on ΔG values), whereas the calibration curves obtained experimentally show a higher sensitivity for 16 carbon chains (Figure 6). This could come from the poor solubility and weak stability of the dyes in purely aqueous medium. Thus, a longer hydrophobic chain would be more sensitive to aggregation induced by LPA addition.

Secondly, regarding the various end groups, i.e., NHS, Silane, and N_3, similar sensitivities were obtained from the calibration curves, whereas the calculated ΔG favor the silane moiety, with −12.1 kcal/mol for Fluo-Silane compared to −3.4 and −3.3 kcal/mol for Fluo-NHS and 16-Azido-FluoLPA, respectively. Moreover, DSHP and Ref-amide were predicted to have a better affinity toward LPA compared to the N_3- and NHS-bearing probes. This suggests that other factors impacting the association of the two molecules (such as those mentioned above) are not accounted for by the simulations.

Nevertheless, experimental and theoretical observations do show an impact of the carbon chain length and of the nature of the end group on the reactivity of these compounds. Developing a simulation model closer to the real system, i.e., several dyes and LPA involved in aggregate formation, for instance, could help improve the agreement between simulated and experimental results.

CONCLUSIONS

The different synthesized fluorescent probes were studied in different solvents, dye, and LPA concentrations. Detailed spectrophotometric characterization allows us to postulate that the fluorescence quenching observed for the band at 610 nm originates from the formation of excimers, a hypothesis supported by time-resolved fluorescence analysis. The change in trend at higher LPA concentrations is not believed to be related to the formation of micelles, given the CMC of LPA several orders of magnitude higher than the concentrations used in this study. A concentration of 0.3 μM for the probes has been identified as optimal in HEPES to prevent the formation of insoluble macroscopic aggregates causing high uncertainties in the measurements. This also increased the sensitivity toward LPA in the nanomolar scale.

The fluorophores bearing a reactive group at the end of the chain have shown the best analytical performance in comparison with the other derivatives. Detection limits of the order of tens of nanomolar were obtained, i.e., significantly lower than those reported previously for this type of probe. In addition, they exhibited good selectivity in the presence of ions and small molecules. The presence of hydrophobic compounds in the sample matrix must however be avoided; nevertheless, the fluorescent probes described herein could be used for total quantification of LPA following the removal of hydrophobic components such as albumin.

EXPERIMENTAL SECTION

Chemicals and Materials. Palmitic acid (≥99%), *N*-hydroxysuccinimide (NHS, 98%), *N*,*N*′-dicyclohexylcarbodiimide (DCC, 99%), diisopropylethylamine (DIPEA, 99.5%), 3-aminopropyltriethoxysilane (APTES, 99%), triethylamine (99%), HEPES (99.5%), boric acid (99.5%), and *N*,*N*-dimethylformamide (DMF, 99.8%) were purchased from Sigma-Aldrich. Dichloromethane (DCM 99.9%), methanol (99.9%), sodium hydroxide (98%), and *o*-phosphoric acid (85%) were purchased from Fisher Scientific; chloroform from (BDH Chemicals); sodium bicarbonate (99.7%) and acetic acid (≥99.7%) from Anachemia; and diethyl ether from Honeywell. Flash column chromatography was performed on a 230−400 mesh silica gel R10030B (Silicycle, Canada).

Instrumentation. Organic compound characterizations were performed using an Agilent DD2 500 MHz NMR and an Agilent 6210 LC-TOF mass spectrometer in electrospray mode. The reaction to form the Fluo-Silane was achieved using a thermomixer (Model Thermomixer C, Eppendorf). Varian Cary spectrophotometers (models 50, 5000 and 7000) were used for the spectrophotometric analysis. Steady-state fluorescence measurements were done on a Jobin-Yvon Fluorolog 3 from Horiba. Time-resolved fluorescence analysis (time-correlated single photon counting, TCSPC) was done on a FluoTime 200 fluorimeter (PicoQuant GmbH) and the generated data were processed with the FluoFit data analysis software from the same supplier. The micellar concentration of LPA was determined using an isothermal titration calorimetry apparatus (Nano ITC, TA Instruments). The pH of buffers was measured with an Accumet Excel XL20 pH meter from Fisher Scientific.

Synthesis of the Probes. The full synthesis scheme used in this study is presented in the Supporting Information, Scheme S1, while the synthetic details of the newly reported compounds are presented below.

Synthesis of Ref-Amide (Compound 10). In a 50 mL round-bottom flask equipped with a stir bar were added 0.48 mmol (0.211 g) of compound **8**, 0.48 mmol (0.123 g) of palmitic acid, 0.48 mmol (0.056 g) of NHS, and 0.71 mmol (0.149 g) of DCC. DMF (25 mL), DCM (5 mL), and DIPEA (1.43 mmol, 251 μL) were then added to initiate the coupling reaction after solubilization using an ultrasonic bath. The reaction mixture was stirred for 1 h in an ice bath followed by 16 h at 25 °C. After solvent removal under reduced pressure, the crude product was purified by column chromatography (silica gel, 9:1 $CHCl_3$/MeOH, Rf = 0.4). Since the NHS eluted at the same time as the product, the fractions were combined and the solvent was evaporated under reduced pressure before transferring the product in a separating funnel with 50 mL of DCM. Liquid−liquid extraction was then performed by washing the organic phase with 2 × 50 mL of H_2O and 2 × 50 mL of brine. The organic phase was separated, dried with $MgSO_4$, filtered under gravity, and evaporated under reduced pressure to obtain 0.100 g of Ref-amide (35% yield). ^{1}H NMR (500 MHz, $CDCl_3$) δ 9.24 (d, J = 6.4 Hz, 2H), 8.77 (s, 1H), 7.77 (d, J = 6.3 Hz, 2H), 7.59 (d, J = 15.9 Hz, 1H), 7.55 (d, J = 8.5 Hz, 2H), 6.89 (d, J = 15.8 Hz, 1H), 6.80 (br, 2H), 4.82 (t, J = 6.8 Hz, 2H), 3.41−3.27 (m, 2H), 3.10 (s, 6H), 2.48−2.22 (m, 4H), 1.62 (p, J = 7.7 Hz, 2H), 1.39−1.12 (m, 30H), 0.87 (t, J = 7.0 Hz, 3H). ^{13}C NMR (126 MHz, $CDCl_3$) δ 175.5, 154.2, 144.2, 142.7, 142.2, 130.8, 122.9, 58.0, 41.5, 36.4, 35.7, 32.1, 31.4, 29.9, 29.86, 29.84, 29.81, 29.75, 29.7, 29.6, 29.5, 26.2, 22.8, 14.3. HRMS (Supporting Information): m/z calcd For $C_{34}H_{54}N_3O^+$: 520.43 $[M]^+$; found, 520.4297.

Synthesis of Fluo-NHS (Compound 16). In a 250 mL round-bottom flask equipped with a stir bar, 1.86 mmol (1.00 g) of compound **15** was dissolved in 200 mL of DCM. In a second 250 mL round-bottom flask was added 1.87 mmol (0.828 g) of compound **8**, which was dissolved in 100 mL of DMF with 4.66 mmol (814 μL) of DIPEA. The content of

https://doi.org/10.1021/acsomega.2c06420
ACS Omega 2023, 8, 1067−1078

each flask was combined in a 500 mL round-bottom flask equipped with a stir bar, and the mixture was stirred at 25 °C for 48 h. This solvent mixture was chosen to allow complete dissolution of the reactants. The solvents were then evaporated under reduced pressure. The NHS residue was removed using liquid−liquid extraction before purifying the remaining crude product by column chromatography following the procedure described below. First, the flask content was dissolved in 100 mL of DCM, transferred to a separating funnel, and washed with 100 mL of H_2O. The aqueous phase was isolated and extracted with 100 mL of DCM to retrieve dyes that were transferred to it. The organic phase, now constituted of 200 mL of DCM, was washed with 100 mL of H_2O, and the formed emulsion was stopped with the addition of 50 mL of brine. The phase separation was allowed to proceed for 1 h before isolating the organic phase and removing the solvent under reduced pressure. The remaining crude was then purified with column chromatography (silica gel, 9:1 DCM/MeOH, Rf = 0.47) with a gradient until 50% MeOH was reached. The fractions containing the product were combined, dried with $MgSO_4$, and filtered on Celite with DCM containing up to 20% MeOH. Solvent evaporation under reduced pressure gave 0.398 g (27% yield) of Fluo-NHS (compound **16**). 1H NMR (500 MHz, CDCl3) δ 9.15 (d, J = 6.3 Hz, 2H), 8.34−8.25 (m, 1H), 7.74 (d, J = 6.1 Hz, 2H), 7.59 (d, J = 15.9 Hz, 1H), 7.52 (d, J = 8.8 Hz, 2H), 6.85 (d, J = 15.8 Hz, 1H), 6.71 (d, J = 8.8 Hz, 2H), 4.78 (br, 2H), 3.36 (br, 2H), 3.09 (s, 6H), 2.83 (br, 5H), 2.59 (t, J = 7.5 Hz, 3H), 2.48−2.24 (m, 5H), 1.73 (p, J = 7.5 Hz, 3H), 1.61 (p, J = 7.8 Hz, 3H), 1.45−1.17 (m, 42H). ^{13}C NMR (126 MHz, CDCl3) δ 144.1, 130.8, 123.1, 51.5, 36.0, 31.3, 29.9, 28.8, 26.5, 25.5, 18.8, 17.5. HRMS (Supporting Information): m/z calcd for $C_{42}H_{63}N_4O_5^+$: 703.48 $[M]^+$; found, 703.4812.

Synthesis of Fluo-Silane (Compound 18). In a 1.5 mL Eppendorf was dissolved 7.1 μmol (0.005 g) of compound **16** in 120 μL of DMF using an ultrasonic bath. Then, 6.8 μmol (1.6 μL) of APTES and 11.4 μmol (1.60 μL) of triethylamine were added. The Eppendorf was stirred in a thermomixer at 25 °C and 1000 RPM for 16 h to generate the Fluo-Silane (compound **18**). HRMS (Supporting Information): m/z calcd for $C_{47}H_{81}N_4O_5Si^+$: 809.60 $[M]^+$; found, 809.6049.

Synthesis of 6-Azido-FluoLPA (Compound 28). In a 10 mL round-bottom flask equipped with a stir bar were added 0.11 mmol (0.050 g) of compound **8**, 0.11 mmol (0.018 g) of compound **20**, 0.12 mmol (0.014 g) of NHS, and 0.15 mmol (0.031 g) of DCC. The powders were dissolved in 5 mL of DMF containing 0.30 mmol (52 μL) of DIPEA. The reaction mixture was stirred for 1 h in an ice bath followed by 48 h at 25 °C. The product was concentrated under reduced pressure before purifying the crude product by column chromatography using a solvent gradient (silica gel, starting at 9:1 $CHCl_3$/MeOH, Rf = 0.18). The fractions containing the product were combined, and the solvent was evaporated under reduced pressure. The product was then dissolved in 30 mL of $CHCl_3$ and washed with 1 × 30 mL saturated sodium bicarbonate. The aqueous phase was extracted with 30 mL of $CHCl_3$ to retrieve dyes that were transferred to it. The organic phases were combined and washed with 2 × 60 mL H_2O and 1 × 60 mL brine. The organic phase was dried with $MgSO_4$ before removing the solvent under reduced pressure. A trituration with diethyl ether allowed the removal of compound **20** residues to obtain 0.008 g (13% yield) of 6-Azido-FluoLPA. ^{1}H NMR (500 MHz, $CDCl_3$) δ 9.23 (br, 2H), 8.96 (br, 1H), 7.83 (br, 2H), 7.66−7.56 (m, 3H), 7.05-6.93 (m, 3H), 4.84 (t, J = 6.8 Hz, 2H), 3.36 (br, 3H), 3.25 (t, J = 6.8 Hz, 3H), 3.12 (s, 6H), 2.47−2.29 (m, 5H), 1.73−1.52 (m, 7H), 1.46−1.38 (m, 3H). ^{13}C NMR (126 MHz, $CDCl_3$) δ 175.2, 169.4, 168.9, 154.5, 152.6, 143.8, 143.5, 133.8, 130.9, 122.5, 116.2, 112.2, 57.9, 40.3, 40.2, 36.6, 35.6, 31.3, 31.1, 29.85, 29.84, 29.81, 29.77, 29.75, 29.72, 29.69, 29.6, 29.5, 29.2, 28.9, 26.1, 25.8, 24.7. HRMS (Supporting Information): m/z calcd for $C_{24}H_{33}N_6O^+$: 421.27 $[M]^+$; found, 421.2792.

Synthesis of 11-Azido-FluoLPA (Compound 29). In a 10 mL round-bottom flask equipped with a stir bar were added 0.11 mmol (0.050 g) of compound **8**, 0.11 mmol (0.026 g) of compound **22**, 0.11 mmol (0.013 g) NHS, and 0.15 mmol (0.031 g) of DCC. The powders were dissolved in 5 mL of DMF containing 0.30 mmol (52 μL) of DIPEA. The reaction mixture was stirred for 1 h in an ice bath followed by 48 h at 25 °C. The product was concentrated under reduced pressure before purifying the crude product with column chromatography using a solvent gradient (silica gel, starting at 9:1 $CHCl_3$/MeOH, Rf = 0.3). The fractions containing the product were combined, and the solvent was evaporated under reduced pressure. The product was then dissolved in 30 mL of $CHCl_3$ and washed with 1 × 30 mL saturated sodium bicarbonate. The organic phase was washed with 2 × 30 mL H_2O and 1 × 30 mL brine before drying with $MgSO_4$ and removing the solvent under reduced pressure. A trituration with diethyl ether allowed the removal of compound **22** residues to obtain 0.011 g (16% yield) of 11-Azido-FluoLPA. ^{1}H NMR (500 MHz, $CDCl_3$) δ 9.30 (d, J = 6.0 Hz, 2H), 8.93 (br, 1H), 7.87 (br, 2H), 7.72−7.59 (m, 3H), 7.04 (m, 3H), 4.85 (br, 2H), 3.37 (br, 3H), 3.24 (t, J = 7.0 Hz, 3H), 3.13 (s, 6H), 2.44−2.30 (m, 5H), 1.69−1.51 (m, 6H), 1.36−1.18 (m, 20H). ^{13}C NMR (126 MHz, $CDCl_3$) δ 175.7, 154.1, 144.3, 130.7, 123.3, 51.6, 36.2, 35.8, 31.4, 29.8, 29.57, 29.55, 29.54, 29.46, 29.3, 29.0, 26.8, 26.1. HRMS (Supporting Information): m/z calcd for $C_{29}H_{43}N_6O^+$: 491.35 $[M]^+$; found, 491.3528.

Synthesis of Fluo-N_3 (Compound 30). In a 10 mL round-bottom flask equipped with a stir bar were added 0.45 mmol (0.201 g) of compound **8** and 0.45 mmol (0.134 g) of compound **27** with 0.442 mmol (0.052 g) of NHS and 0.58 mmol (0.121 g) of DCC. The powders were dissolved in 6 mL of DMF containing 1.16 mmol (204 μL) of DIPEA. The reaction mixture was stirred for 1 h in an ice bath followed by 48 h at 25 °C. The product was concentrated under reduced pressure before purifying the crude product by column chromatography using a solvent gradient (silica gel, starting at 9:1 $CHCl_3$/MeOH, Rf = 0.38). The fractions containing the product were combined, and the solvent was evaporated under reduced pressure. The product was then dissolved in 50 mL of DCM and washed with 3 × 50 mL of H_2O and 1 × 10 mL brine to remove residual NHS. The organic phase was dried with $MgSO_4$ before removing the solvent under reduced pressure to obtain 0.096 g (33% yield) of Fluo-N_3 (compound **30**). ^{1}H NMR (500 MHz, $CDCl_3$) δ 9.24 (d, J = 6.4 Hz, 2H), 8.72 (br, 1H), 7.78 (d, J = 6.4 Hz, 2H), 7.60 (d, J = 15.9 Hz, 1H), 7.56 (d, J = 8.7 Hz, 2H), 6.91 (d, J = 15.9 Hz, 1H), 6.85 (d, J = 8.5 Hz, 2H), 4.82 (t, J = 6.8 Hz, 2H), 3.36 (br, 2H), 3.26 (t, J = 7.0 Hz, 3H), 3.11 (s, 6H), 2.40−2.29 (m, 5H), 1.66−1.54 (m, 6H), 1.37−1.19 (m, 32H). ^{13}C NMR (126 MHz, $CDCl_3$) δ 175.5, 154.2, 144.1, 130.8, 122.9, 58.0, 51.7, 41.4, 36.4, 35.7, 31.4, 29.81, 29.80, 29.77, 29.72, 29.69, 29.6, 29.55, 29.3, 29.0, 26.9, 26.2. HRMS (Supporting Information): m/z calcd for $C_{34}H_{53}N_6O^+$: 561.43 $[M]^+$; found, 561.4317.

https://doi.org/10.1021/acsomega.2c06420
ACS Omega 2023, 8, 1067−1078

Stock Solutions. A stock 0.1 M HEPES buffer (pH 7.4) was prepared by dissolution of 2.38 g of HEPES in 80 mL of Milli-Q water. The pH was adjusted to 7.4 with sodium hydroxide before completing the volume to 100 mL with Milli-Q water. A 10-fold dilution produced the 10 mM stock solution used to prepare the various LPA solutions.

For titrations with LPA, a 1 mM LPA solution in 10 mM HEPES buffer was prepared and incremental volume additions were performed directly in the cell containing the dyes.

To ensure complete dissolution of the dyes, stock solutions were prepared in MeOH (0.5 mM for Ref-amide, Fluo-NHS, Fluo-Silane, Fluo-N_3, 6-AzidoFluoLPA and 11-AzidoFluoLPA) except for DSHP to match the conditions of the paper from Zhao et al. in EtOH (1 mM in EtOH).[34]

To study the effect of pH on probes interaction with LPA, Britton−Robinson buffers containing 40 mM H_3PO_4, 40 mM CH_3COOH, and 40 mM H_3BO_3 were prepared according to the following procedure. Boric acid was dissolved in Milli-Q water to obtain a 0.5 M stock solution, and acetic acid and phosphoric acid were diluted to produce 2 M stock solutions. In a 150 mL beaker equipped with a magnetic stirrer, 40 mL of Milli-Q water was added followed by the addition of 8 mL of boric acid solution and 2 mL of acetic acid and phosphoric acid solution. While monitoring pH, the mixture was titrated with sodium hydroxide until the desired pH was reached. Milli-Q water was added to reach a total volume of 100 mL in a volumetric flask. This procedure was repeated for every pH needed, and the measured pH values of the final buffer solutions are presented in the Supporting Information (Table S1).

For the selectivity and interference experiments, stock solutions of 1 mM for the ions and small molecules were obtained from the dilution of prepared 50 mM solutions in 10 mM HEPES buffer, pH 7.4. The BSA solution used was at 1 mg/mL. The structurally similar compounds (1 mM) were prepared in methanol to ensure their solubility. Interfering species (3 μL) were added to reach a concentration of 1 μM (except for BSA, 1 μg/mL) in the cell containing 0.3 μM of the studied probes.

Computational Details. All of the calculations were performed on the full structures of the reported compounds. Calculations were performed with the GAUSSIAN 16 suite of programs.[36] The ωB97XD functional[37] was qualified as promising by Grimme[38] and was chosen as a good general functional for organic molecules. It was used in combination with the 6-311G(d,p) basis set for all atoms.[39] We used implicit solvation effects included with the SMD[40] method (solvent = water) for all calculations. The stationary points were characterized as minima by full vibration frequency calculations (no imaginary frequency). All geometry optimizations were carried out without any symmetry constraints. The Cartesian coordinates of all structures are fully detailed in the Supporting Information (Figures S17−S33).

■ ASSOCIATED CONTENT

Supporting Information

The Supporting Information is available free of charge at https://pubs.acs.org/doi/10.1021/acsomega.2c06420.

Complete synthesis scheme; NMR characterization data for compounds **10,16, 28, 29**, and **30**; critical micellar concentration of LPA in the analysis medium used; spectrophotometric study of the effect of dye concentration and with the addition of LPA; fluorescence lifetime of Fluo-Silane and the effect of solvent polarity on dyes spectral properties; dye−LPA interaction kinetics and effect of pH; selectivity and interference studies of Fluo-Silane and Fluo-N_3; DFT structure coordinates; and other references (PDF)

■ AUTHOR INFORMATION

Corresponding Author

Denis Boudreau − *Department of Chemistry, Université Laval, Québec, Canada G1V 0A6; Center for Optics, Photonics and Lasers, Université Laval, Québec, Canada G1V 0A6;* orcid.org/0000-0001-5152-2464; Email: denis.boudreau@chm.ulaval.ca

Authors

Nicolas Fontaine − *Department of Chemistry, Université Laval, Québec, Canada G1V 0A6; Center for Optics, Photonics and Lasers, Université Laval, Québec, Canada G1V 0A6;* Present Address: Department of Chemistry, Université de Sherbrooke, Sherbrooke, Quebec, Canada J1K 2R1; orcid.org/0000-0001-7623-475X

Lara Harter − *Department of Chemistry, Université Laval, Québec, Canada G1V 0A6; Center for Optics, Photonics and Lasers, Université Laval, Québec, Canada G1V 0A6*

André Marette − *Quebec Heart and Lung Institute, Université Laval, Québec, Canada G1V 4G5; Institute of Nutrition and Functional Foods, Université Laval, Québec, QC, Canada G1V 0A6*

Complete contact information is available at: https://pubs.acs.org/10.1021/acsomega.2c06420

Author Contributions

N.F.: methodology, experiments, analysis, and writing. L.H.: computational analysis, experiments, and writing. A.M.: supervision, funding, and conceptualization. D.B.: supervision, funding, conceptualization, and reviewing. All authors have given approval to the final version of the manuscript.

Notes

The authors declare no competing financial interest.

■ ACKNOWLEDGMENTS

This research was supported by the Sentinel North program of Université Laval, made possible, in part, by funding from the Canada First Research Excellence Fund. Other sources of financial support include the National Science and Engineering Research Council of Canada (NSERC), le Fonds de recherche du Québec—Nature et technologies (FRQ-NT) and Innovation Canada. The authors acknowledge Audrey Picard-Lafond, Ph.D., for insightful discussions on the synthesis and experimental results as well as Vincent Desrosiers, Ph.D. candidate, and Prof. Guillaume Bélanger-Chabot for their help with computational analysis interpretation.

■ REFERENCES

(1) Califf, R. M. Biomarker Definitions and Their Applications. *Exp. Biol. Med.* **2018**, *243*, 213−221.
(2) Aronson, J. K.; Ferner, R. E. Biomarkers - A General Review. *Curr. Protoc. Pharmacol.* **2017**, *76*, 9.23.1−9.23.27.
(3) Wishart, D. S. Metabolomics for Investigating Physiological and Pathophysiological Processes. *Physiol. Rev.* **2019**, *99*, 1819−1875.
(4) Schmidt, D. R.; Patel, R.; Kirsch, D. G.; Lewis, C. A.; Vander Heiden, M. G.; Locasale, J. W. Metabolomics in Cancer Research and

Emerging Applications in Clinical Oncology. *CA-Cancer J. Clin.* **2021**, *71*, 333−358.
(5) Nimse, S. B.; Sonawane, M. D.; Song, K. S.; Kim, T. Biomarker Detection Technologies and Future Directions. *Analyst* **2016**, *141*, 740−755.
(6) Chiu, C. Y.; Miller, S. A. Clinical Metagenomics. *Nat. Rev. Genet.* **2019**, *20*, 341−355.
(7) Echle, A.; Rindtorff, N. T.; Brinker, T. J.; Luedde, T.; Pearson, A. T.; Kather, J. N. Deep Learning in Cancer Pathology: A New Generation of Clinical Biomarkers. *Br. J. Cancer* **2021**, *124*, 686−696.
(8) Broza, Y. Y.; Zhou, X.; Yuan, M.; Qu, D.; Zheng, Y.; Vishinkin, R.; Khatib, M.; Wu, W.; Haick, H. Disease Detection with Molecular Biomarkers: From Chemistry of Body Fluids to Nature-Inspired Chemical Sensors. *Chem. Rev.* **2019**, *119*, 11761−11817.
(9) Vogt, W. Pharmacologically Active Acidic Phospholipids and Glycolipids. *Biochem. Pharmacol.* **1963**, *12*, 415−420.
(10) Pagès, C.; Simon, M. F.; Valet, P.; Saulnier-Blache, J. S. Lysophosphatidic Acid Synthesis and Release. *Prostaglandins Other Lipid Mediators* **2001**, *64*, 1−10.
(11) Lin, M. E.; Herr, D. R.; Chun, J. Lysophosphatidic Acid (LPA) Receptors: Signaling Properties and Disease Relevance. *Prostaglandins Other Lipid Mediators* **2010**, *91*, 130−138.
(12) Baker, D. L.; Desiderio, D. M.; Miller, D. D.; Tolley, B.; Tigyi, G. J. Direct Quantitative Analysis of Lysophosphatidic Acid Molecular Species by Stable Isotope Dilution Electrospray Ionization Liquid Chromatography-Mass Spectrometry. *Anal. Biochem.* **2001**, *292*, 287−295.
(13) Moolenaar, W. H. Lysophosphatidic Acid, a Multifunctional Phospholipid Messenger. *J. Biol. Chem.* **1995**, *270*, 12949−12952.
(14) Deng, W.; Balazs, L.; Wang, D. A.; Van Middlesworth, L.; Tigyi, G.; Johnson, L. R. Lysophosphatidic Acid Protects and Rescues Intestinal Epithelial Cells from Radiation- and Chemotherapy-Induced Apoptosis. *Gastroenterology* **2002**, *123*, 206−216.
(15) Lapierre, D. M.; Tanabe, N.; Pereverzev, A.; Spencer, M.; Shugg, R. P. P.; Dixon, S. J.; Sims, S. M. Lysophosphatidic Acid Signals through Multiple Receptors in Osteoclasts to Elevate Cytosolic Calcium Concentration, Evoke Retraction, and Promote Cell Survival. *J. Biol. Chem.* **2010**, *285*, 25792−25801.
(16) Aoki, J.; Inoue, A.; Okudaira, S. Two Pathways for Lysophosphatidic Acid Production. *Biochim. Biophys. Acta, Mol. Cell Biol. Lipids* **2008**, *1781*, 513−518.
(17) Sedláková, I.; Vávrová, J.; Tošner, J.; Hanousek, L. Lysophosphatidic Acid (LPA) - A Perspective Marker in Ovarian Cancer. *Tumor Biol.* **2011**, *32*, 311−316.
(18) Xu, Y.; Shen, Z.; Wiper, D. W.; Wu, M.; Morton, R. E.; Elson, P.; Kennedy, A. W.; Belinson, J.; Markman, M.; Casey, G. Lysophosphatidic Acid as a Potential Biomarker for Ovarian and Other Gynecologic Cancers. *J. Am. Med. Assoc.* **1998**, *280*, 719−723.
(19) Hosogaya, S.; Yatomi, Y.; Nakamura, K.; Ohkawa, R.; Okubo, S.; Yokota, H.; Ohta, M.; Yamazaki, H.; Koike, T.; Ozaki, Y. Measurement of Plasma Lysophosphatidic Acid Concentration in Healthy Subjects: Strong Correlation with Lysophospholipase D Activity. *Ann. Clin. Biochem.* **2008**, *45*, 364−368.
(20) Rahman, M. A.; Haron, D. E. M.; Hollows, R. J.; Ghani, Z. D. F. A.; Mohd, M. A.; Chai, W. L.; Ng, C. C.; Lye, M. S.; Karsani, S. A.; Yap, L. F.; Paterson, I. C. Profiling Lysophosphatidic Acid Levels in Plasma from Head and Neck Cancer Patients. *PeerJ* **2020**, *8*, No. e9304.
(21) Kano, K.; Matsumoto, H.; Kono, N.; Kurano, M.; Yatomi, Y.; Aoki, J. Suppressing Postcollection Lysophosphatidic Acid Metabolism Improves the Precision of Plasma LPA Quantification. *J. Lipid Res.* **2021**, *62*, No. 100029.
(22) Wang, J.; Sibrian-Vazquez, M.; Escobedo, J. O.; Lowry, M.; Wang, L.; Chu, Y. H.; Moore, R. G.; Strongin, R. M. Simple Enrichment and Analysis of Plasma Lysophosphatidic Acids. *Analyst* **2013**, *138*, 6852−6859.
(23) Jesionowska, A.; Cecerska, E.; Dolegowska, B. Methods for Quantifying Lysophosphatidic Acid in Body Fluids: A Review. *Anal. Biochem.* **2014**, *453*, 38−43.
(24) Wen, Y.; Huo, F.; Yin, C. Organelle Targetable Fluorescent Probes for Hydrogen Peroxide. *Chin. Chem. Lett.* **2019**, *30*, 1834−1842.
(25) Yang, Y.; Zhou, T.; Jin, M.; Zhou, K.; Liu, D.; Li, X.; Huo, F.; Li, W.; Yin, C. Thiol-Chromene "Click" Reaction Triggered Self-Immolative for NIR Visualization of Thiol Flux in Physiology and Pathology of Living Cells and Mice. *J. Am. Chem. Soc.* **2020**, *142*, 1614−1620.
(26) Xu, M.; Kelley, S. P.; Glass, T. E. A Multi-Component Sensor System for Detection of Amphiphilic Compounds. *Angew. Chem., Int. Ed.* **2018**, *57*, 12741−12744.
(27) Yue, Y.; Huo, F.; Ning, P.; Zhang, Y.; Chao, J.; Meng, X.; Yin, C. Dual-Site Fluorescent Probe for Visualizing the Metabolism of Cys in Living Cells. *J. Am. Chem. Soc.* **2017**, *139*, 3181−3185.
(28) Morita, S. Y.; Ueda, K.; Kitagawa, S. Enzymatic Measurement of Phosphatidic Acid in Cultured Cells. *J. Lipid Res.* **2009**, *50*, 1945−1952.
(29) Yao, D.; Lin, Z.; Wu, J. Near-Infrared Fluorogenic Probes with Polarity-Sensitive Emission for in Vivo Imaging of an Ovarian Cancer Biomarker. *ACS Appl. Mater. Interfaces* **2016**, *8*, 5847−5856.
(30) Zheng, Z.; Geng, W. C.; Gao, J.; Wang, Y. Y.; Sun, H.; Guo, D. S. Ultrasensitive and Specific Fluorescence Detection of a Cancer Biomarker: Via Nanomolar Binding to a Guanidinium-Modified Calixarene. *Chem. Sci.* **2018**, *9*, 2087−2091.
(31) de la Franier, B.; Thompson, M. Detection of the Ovarian Cancer Biomarker Lysophosphatidic Acid in Serum. *Biosensors* **2020**, *10*, No. 13.
(32) Hu, B.; Wu, P. An Ultrathin Polydiacetylene Nanosheet as Dual Colorimetric and Fluorescent Indicator for Lysophosphatidic Acid, a Cancer Biomarker. *Giant* **2020**, *3*, No. 100025.
(33) Chen, K. H.; Yang, J. S.; Hwang, C. Y.; Fang, J. M. Phospholipid-Induced Aggregation and Anthracene Excimer Formation. *Org. Lett.* **2008**, *10*, 4401−4404.
(34) Zhao, W.; Liu, W.; Zhang, W.; Zeng, L.; Fan, Z.; Wu, J.; Wang, P. A Chromo- and Fluorogenic Sensor for Probing the Cancer Biomarker Lysophosphatidic Acid. *Analyst* **2012**, *137*, 1853−1859.
(35) Jiang, T.; Lu, N.; Yang, J.; Hang, Y.; Wang, J.; Zhao, P.; Hua, J. Dibenzo[a,c]Phenazine-Derived near-Infrared Fluorescence Biosensor for Detection of Lysophosphatidic Acid Based on Aggregation-Induced Emission. *RSC Adv.* **2015**, *5*, 102863−102867.
(36) Frisch, M. J.; Trucks, G. W.; Schlegel, H. B.; Scuseria, G. E.; Robb, M. A.; Cheeseman, J. R.; Scalmani, G.; Barone, V.; Petersson, G. A.; Nakatsuji, H.; Li, X.; Caricato, M.; Marenich, A. V.; Bloino, J.; Janesko, B. G.; Gomperts, R.; Mennucci, B.; Hratchian, H. P.; Ortiz, J. V.; Izmaylov, A. F.; Sonnenberg, J. L.; Williams-Young, D.; Ding, F.; Lipparini, F.; Egidi, F.; Goings, J.; Peng, B.; Petrone, A.; Henderson, T.; Ranasinghe, D.; Zakrzewski, V. G.; Gao, J.; Rega, N.; Zheng, G.; Liang, W.; Hada, M.; Ehara, M.; Toyota, K.; Fukuda, R.; Hasegawa, J.; Ishida, M.; Nakajima, T.; Honda, Y.; Kitao, O.; Nakai, H.; Vreven, T.; Throssell, K.; Montgomery, J. A., Jr.; Peralta, J. E.; Ogliaro, F.; Bearpark, M. J.; Heyd, J. J.; Brothers, E. N.; Kudin, K. N.; Staroverov, V. N.; Keith, T. A.; Kobayashi, R.; Normand, J.; Raghavachari, K.; Rendell, A. P.; Burant, J. C.; Iyengar, S. S.; Tomasi, J.; Cossi, M.; Millam, J. M.; Klene, M.; Adamo, C.; Cammi, R.; Ochterski, J. W.; Martin, R. L.; Morokuma, K.; Farkas, O.; Foresman, J. B.; Fox, D. J.*Gaussian 16*, revision C.01; Gaussian, Inc.: Wallingford CT, 2016.
(37) Chai, J.-D.; Head-Gordon, M. Long-Range Corrected Hybrid Density Functionals with Damped Atom-Atom Dispersion Corrections. *Phys. Chem. Chem. Phys.* **2008**, *10*, 6615−6620.
(38) Goerigk, L.; Grimme, S. A Thorough Benchmark of Density Functional Methods for General Main Group Thermochemistry, Kinetics, and Noncovalent Interactions. *Phys. Chem. Chem. Phys.* **2011**, *13*, 6670−6688.
(39) Krishnan, R.; Binkley, J. S.; Seeger, R.; Pople, J. A. Self-Consistent Molecular Orbital Methods. XX. A Basis Set for Correlated Wave Functions. *J. Chem. Phys.* **1980**, *72*, 650−654.
(40) Marenich, A. V.; Cramer, C. J.; Truhlar, D. G. Universal Solvation Model Based on Solute Electron Density and on a Continuum Model of the Solvent Defined by the Bulk Dielectric

https://doi.org/10.1021/acsomega.2c06420
ACS Omega 2023, 8, 1067−1078

Constant and Atomic Surface Tensions. *J. Phys. Chem. B* **2009**, *113*, 6378−6396.
(41) Li, S. H.; Xu, X.; Zhou, Y.; Zhao, Q.; Liu, Y. Reversibly Tunable White-Light Emissions of Styrylpyridiniums with Cucurbiturils in Aqueous Solution. *Org. Lett.* **2017**, *19*, 6650−6653.
(42) Bains, G. K.; Kim, S. H.; Sorin, E. J.; Narayanaswami, V. The Extent of Pyrene Excimer Fluorescence Emission Is a Reflector of Distance and Flexibility: Analysis of the Segment Linking the LDL Receptor-Binding and Tetramerization Domains of Apolipoprotein E3. *Biochemistry* **2012**, *51*, 6207−6219.
(43) Mishra, A.; Behera, G. B.; Krishna, M. M. G.; Periasamy, N. Time-Resolved Fluorescence Studies of Aminostyryl Pyridinium Dyes in Organic Solvents and Surfactant Solutions. *J. Lumin.* **2001**, *92*, 175−188.
(44) Zhang, T.; Brantley, S. L.; Verreault, D.; Dhankani, R.; Corcelli, S. A.; Allen, H. C. Effect of PH and Salt on Surface PKa of Phosphatidic Acid Monolayers. *Langmuir* **2018**, *34*, 530−539.
(45) Myers, D.*Surfaces, Interfaces, and Colloids: Principles and Applications*, 2nd ed.; John Wiley & Sons, Inc., 2002.
(46) Gerrard, J. M.; Kindom, S. E.; Peterson, D. A.; Peller, J.; Krantz, K. E.; White, J. G. Lysophosphatidic Acids Influence on Platelet Aggregation and Intracellular Calcium Flux. *Am. J. Pathol.* **1979**, *96*, 423−438.

https://doi.org/10.1021/acsomega.2c06420
ACS Omega 2023, 8, 1067−1078